Accepted Manuscript

Authors: María V. Morales, Kinga Góra-Marek, Hermen Musch, Antonio Pineda, Blaine Murray, Stelios Stefanidis, Lorena Falco, Karolina Tarach, Ekaterina Ponomareva, Jan Henk Marsman, Ignacio Melián-Cabrera

Advanced oxidation process for coke removal: A systematic study of hydrogen peroxide and OH-derived-Fenton radicals of a fouled zeolite

María V. Morales,[a,b‡*] Kinga Góra-Marek,[c‡] Hermen Musch,[d‡] Antonio Pineda,[a] Blaine Murray,[a] Stelios Stefanidis,[a] Lorena Falco,[a] Karolina Tarach,[c] Ekaterina Ponomareva,[e] Jan Henk Marsman,[f] Ignacio Melián-Cabrera [a,d]

[a.] European Bioenergy Research Institute (EBRI), School of Engineering and Applied Science, Aston University, Aston Triangle, Birmingham, B4 7ET, United Kingdom.

[b.] CNRS-CEMHTI, 1D Av. de la Recherche Scientifique CS 90055, 45071 Orléans Cedex 2, France.

[c.] Faculty of Chemistry, Jagiellonian University in Kraków, 2 Gronostajowa St., 30-387 Kraków, Poland.

[d.] Chemical Reaction Engineering (ITM), Faculty of Science and Engineering, University of Groningen, Nijenborgh 4, 9747 AG Groningen, The Netherlands.

[e.] Semenov Institute of Chemical Physics, Department of Kinetics and Catalysis, Laboratory of Heterogeneous Catalysis, Russian Academy of Sciences, 119991 Moscow, Russian Federation.

[f.] Analytical & Instrumental Analysis Department (ITM), Faculty of Science and Engineering, University of Groningen, Nijenborgh 4, 9747 AG Groningen, The Netherlands.

[‡] Equal contribution.

* Corresponding Author:

marivi.morales@cnrs-orleans.fr (María V. Morales)

Graphical abstract
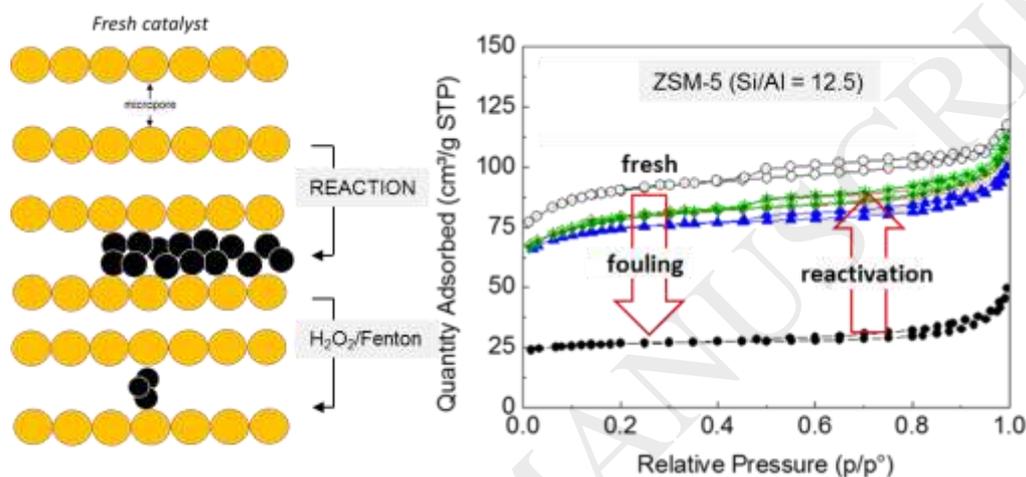
Highlights

- Advanced oxidation processes have been applied on a coked zeolite.
- Structure and texture were preserved, while acidity was improved.
- Complete catalyst activity recovery was achieved.
- Water treatment, followed by H_2O_2 and finally Fenton process are recommended as methodology guidelines.

Abstract

The regeneration process of a fouled catalyst typically involves treatments at high temperature which often cause irreversible damages on the catalyst's properties. In this work, Fenton

chemistry-derived $^{\bullet}OH$ species, and H_2O_2, are proposed as oxidizing agents to reactivate a porous catalyst at mild conditions, below 100 °C. The chosen catalyst is a microporous ZSM-5 zeolite, which is a challenging candidate due to the mass transfer limitations with possible recombination of the hydroxyl radicals; thereby being an obstacle to oxidize organics occluded in the micropores. The organics deposition over a ZSM-5 zeolite during the *D*-glucose dehydration reaction was confirmed by a number of characterization techniques, which revealed a considerable decrease in the surface area, pore volume and acid site density in the fouled catalyst. By properly selecting the regeneration conditions, reactivation via Fenton or H_2O_2 was highly effective in terms of removal of the organics as well as recovery of the initial catalytic activity. The properties of the H_2O_2 treated-zeolite, the optimal treatment in this case study, were preserved with similar structural and textural features and improved acidity. Hot water extraction was ineffective to remove the humins from ZSM-5. Mechanistically, the presence of Fe impurities in the zeolite structure did not allow to discriminate between a homo, heterogeneous, or a direct H_2O_2 pathway, or a combination of them. The exhibited conversion by the regenerated zeolite was comparable to that of the fresh one.

1. Introduction

Catalyst stability and deactivation are possibly the most crucial properties in a catalyst development program. Deactivation occurs by a number of different chemical and physical mechanisms. These include: poisoning, thermal sintering or loss of metal active surface area, mechanical failure, chemical degradation and coking, the latter is more generally known as fouling [1-4].

Fouling is the physical deposition of organic compounds from the fluid phase on the catalyst surface, which results in activity loss. Fouling affects the catalyst performance in various manners by strong chemisorption, forming organic-based multilayers which prevent reactants from accessing active sites, both at the surface and within the pores. These organics can encapsulate active nanoparticles leading to deactivation. In the case of porous catalytic materials, the surface area and pore volume will be progressively diminished, as the reaction proceeds, with a sharp drop in yield when the pores are fully fouled with such organics. The characteristic feature with this process lays on the fact that fouling kinetics may vary from a few seconds to several years depending on the process, catalyst and process conditions [4].

The regeneration of a fouled catalyst is conventionally carried out through oxidation in air or O_2, requiring temperatures between 400 and 600 °C [3], conditions that are favourable for metal sintering and surface area depletion by coarsening or aggregation. In some occasions, regeneration temperatures as high as 700 °C have been reported [5]. In the case of Al-containing zeolites, the steam produced during the reactivation in combination with the high reactivation temperatures, create extra-framework Al [6]. This phenomenon progressively reduces the Brønsted acid sites after each reactivation cycle. In practical terms, the thermal reactivation is energy intensive and the produced vapours corrode equipment gradually and irreversibly. Therefore ways to reactivate fouled porous catalysts at milder conditions will have significant capital and operational savings, as well as preserve the properties of the catalyst for a longer service time. The benefits are twofold, from the process and catalyst point of views. Typically, alternative approaches have focused on faster treatments at lower temperatures such as ozone [7,8] or non-thermal plasma [9,10], to cite the most successful examples. Liquid-phase treatments requiring simpler hardware and mild conditions are hardly reported.

The Fenton reaction consists of the generation of $^{\bullet}OH$ species from H_2O_2 in the presence of a Fe salt; this acts as catalyst in a Fe^{3+}/Fe^{2+} redox cycle as shown in reactions 1 and 2. This

process is very sensitive to the reaction conditions, leading to undesired pathways such as reactions 3 and 4 where hydroxyl radicals are wasted. A benefit of this oxidative route is that the radicals can be produced at low temperature (<100 °C). Therefore it can be applied in a wide range of situations, from contaminated waste water [11] to soils [12]. The second benefit is a very-high oxidation potential: 2.80 V as compared to 1.77 V for H_2O_2 [13]. Not surprisingly this technology has been employed to mineralize waste water, since most of the organic compounds from industrial waste streams can effectively be oxidized.

$$H_2O_2 + Fe^{3+} \rightarrow HO_2^{\bullet} + H^+ + Fe^{2+} \tag{1}$$

$$H_2O_2 + Fe^{2+} \rightarrow {}^{\bullet}OH + OH^- + Fe^{3+} \tag{2}$$

$${}^{\bullet}OH + Fe^{2+} \rightarrow OH^- + Fe^{3+} \tag{3}$$

$${}^{\bullet}OH + H_2O_2 \rightarrow HO_2^{\bullet} + H_2O \tag{4}$$
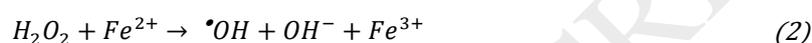
This approach was also very effective in a different application; as a mild detemplation to decompose the structural organic directing agent of zeolites and mesoporous materials, such as beta zeolite [14-17], MCM-41 [18], SBA-15 [19,20], mesoporous colloidal silica [21], mesoporous silicates and aluminosilicates [22,23], RUB-18 [24], aluminophosphates [25,26], silicalite-1 colloids, and films containing zeolite nanoparticles [27]. In this way, thermal calcination was avoided leading to benefits in terms of higher pore volume, better structural preservation, improved intrawall connectivity or higher acidity of the materials produced in this manner.

In this work, Fenton chemistry driven ${}^{\bullet}OH$ have been applied to reactivate a fouled fully microporous material. A fouled microporous material is kinetically challenging. The hydroxyl radical's life time is relatively short, while the diffusional coefficients for mass transport in a zeolite crystal are very small. Therefore under such situation the likelihood of ${}^{\bullet}OH$ recombination is high, leading to poor oxidation performances. A few studies can be found in literature dealing with the application of Fenton chemistry on a fouled zeolite, achieving

moderate or null reactivation efficiencies. For example, Wang *et al* report 60% recovery of the adsorption capacity of a methylene blue fouled MCM-22 [28], while Braschi *et al* found no effect of the Fenton treatment on a sulphonamide-polluted zeolite Y [29]. An interesting study by Chiu and co-workers [30] describes the regeneration of activated carbon, pre-saturated with phenol and Suwannee River natural organic matter (NOM); they report high regeneration efficiencies. However, textural data for the fresh and deactivated materials were not provided to understand the good results obtained at room temperature. From the innovation view point, this is the first report describing the reactivation of a fouled catalyst using the Fenton chemistry as well as reporting in detail the characterization data of the fresh and reactivated catalyst. Regeneration of a fouled catalyst, in particular a microporous zeolite, in which the organic deposition takes place alongside such a restricted porous network, is a challenging case study from an academic point of view.

One of the key aspects that is poorly understood about the Fenton chemistry is the fact that selecting the appropriate reaction conditions is very critical [31]. If this is not done properly, the $^{\bullet}$OH species are not effectively used. For instance, conditions applied to contaminated waste water cannot be directly applied to soils. In this study, by carefully defining the reactions conditions, reactivation efficiencies higher than 95%, with practically total recovery of the initial activity of a microporous ZSM-5 catalyst, have been achieved. The properties of the fresh, deactivated and reactivated catalysts were evaluated showing structural, acidic and textural preservation of the reactivated catalysts.

2. Experimental

2.1 Materials

Chemicals were purchased from commercial suppliers and used directly without additional

purification:

2.1.1 Fenton reaction

Stabilized hydrogen peroxide (30 % (w/w) H_2O_2 in H_2O) was purchased from Merck (ref. 107209). Stabilized H_2O_2, which is usually of relatively high concentrations, is acidic in order to have maximum stability which minimizes its decomposition under normal storage and handling conditions. $Fe(NO_3)_3 \cdot 9H_2O$ (98 %, metal basis, denoted as Fe(III)-nitrate) from Riedel-de-Haën; and HNO_3 from Merck ($\geq$ 65 % (w/w)).

2.1.2 Chemicals and materials involved in the dehydration of *D*-glucose reaction

D-Glucose (99.5 % (w/w)) was purchased from Sigma Life Science; sulphuric acid (95-97 % (w/w), pro analysis) from Merck; formic acid (98 % (w/w)) and levulinic acid (98 % (w/w)) were purchased from Sigma Aldrich. The NH_4-ZSM-5 zeolite was kindly supplied by Süd-Chemie (Clariant); it is an Alsi-Penta no. 27 with Si/Al = 12.5.

2.2 Zeolite activation

The protonic zeolite form was prepared from the NH_4-form by ammonia desorption. The general calcination procedure was carried out in a LT9/11 Nabertherm box furnace. The samples were loaded in porcelain crucibles in shallow bed configuration, heated from 30 to 550 °C at 5 °C/min and held at 550 °C for 6 h. The proton form of the zeolite is denoted as AP27-F.

2.3 Catalytic tests

Ace^TM- pressure tubes: A solution of 0.125 M D-Glucose was prepared in large quantity, and then 3 ml was added to each of the 10 ml thick-wall glass Ace pressure tubes used as reactors. In each tube, 0.15 g of activated ZSM-5 was loaded and a conical, magnetic stir bar was added after. The tubes were sealed with screw-on caps. Four of such tubes were processed in one experimental run.

The four tubes were simultaneously transferred to an aluminium block with holes sized to accommodate the tubes. The aluminium block was immersed in an oil bath maintained at the desired temperature of 180 °C. After 1.5, 3, 4.5 and 6 h, one of the tubes was removed and quenched in an ice bath, one at a time.

After quenching, part of the liquid solution was withdrawn using a syringe fitted with a 0.45 μm filter. The composition of the liquid fraction of the reaction medium was determined by HPLC. The HPLC apparatus consists of a Hewlett Packard 1050 pump, a Bio-Rad organic acid column Aminex HPX-87H operated at 60 °C and a Waters 410 differential refractive index detector. An aqueous mobile phase solution of 5 mM sulphuric acid was used at a flow rate of 0.55 cm^3/min. An analysis time of 40 minutes was chosen as the main reactants and products were separated within this run time. External calibration was performed. Reference solutions containing known concentrations of glucose, formic acid and levulinic acid were used to prepare calibration curves that were used to determine the concentration of these products in the quenched solution. The remaining contents of the quenched tubes were washed with 20 ml milli-Q water and centrifuged. The resulting solids were further dried for two days in air at 70 °C. In this way four brownish spent catalyst samples were obtained and stored in sealed bottles.

Autoclave experiments: To create more deactivated catalyst the reaction was scaled up by using a 100 mL-autoclave reactor. In a Teflon-lined autoclave, 40 ml of a 0.125 M glucose solution was added together with 2.0 g of ZSM-5. The autoclave was immersed in an oil bath already maintained at a temperature of 180 °C. After 6 h, the autoclave was removed from the oil bath and cooled down by putting it in ice. The suspension was filtered and washed with 50 mL demineralised water and dried at 70 °C in a stove oven for two days.

Reference material: Instead of using 2.0 g ZSM-5, a solution of 0.125 M sulphuric acid is used, using the autoclave to produce a H_2SO_4 catalysed reference humin material.

2.4 Catalyst reactivation

Fenton reactivation: 0.2 g of deactivated material was mixed with 6 mL of 30% *wt.* H_2O_2 (stabilized) in an Ace pressure tube and stirred until the mixture became homogeneous. Then, the chosen concentration of Fe was adjusted. In the standard experiment 30 mg Fe/Kg solution (referred to ppm) was used. This concentration was obtained by adding 200 μl of a stock solution (0.5425 g Fe(III)-nitrate in 100 mL of deionised water). The flask containing the reaction mixture was equipped with a small magnetic stirrer and closed with a stopper with a small hole for releasing pressure generated from the decomposition gases. The flask was submerged in a preheated oil bath at the desired temperature (*e.g.* 70 or 90 °C) and was maintained for 20 h under stirring. Fig. S-1 shows the employed set-up. The catalyst was separated by centrifugation, washed with milli-Q water and dried overnight at 80 °C in an oven.

Non-Fenton treatment: The experiments were similar to the Fenton counterparts without adding any Fe salt. The pH was regulated to be similar.

Treatment in hot water: This is a reference experiment to understand if the coke organics in the catalyst are soluble in hot water. Therefore, instead of using H_2O_2, hot water (milli-Q) was used following the above described experimental steps.

The starting and derived materials with their corresponding treatment and codes are summarized in Table 1.

2.5 Characterization methods

2.5.1 Thermogravimetric analysis

Thermogravimetric analyses (TGA) were carried out in a Mettler-Toledo (TGA/SDTA851e) analyser using a flow of synthetic air. Crucibles made of α-alumina were filled with 10-15 mg

of sample. The samples were heated from 30 to 900 °C at a heating rate of 10 °C/min in a flow of synthetic air of 80 mL/min (NTP). A correction was made by subtracting the mass profile of an empty crucible from the measured weight of a sample.

2.5.2 Nitrogen physisorption

Textural analyses of the fresh, deactivated, and regenerated catalysts were analysed by N_2-physisorption at -196 °C using a Micromeritics ASAP 2020 instrument. Prior to the measurements, the samples were outgassed under vacuum at 300 °C for 6 h. The Fenton-derived and deactivated catalysts were degassed at 150 °C to ensure that the humin deposit was unimpaired. The surface area was calculated by BET method (S_{BET}). The single point pore volume (V_T) was estimated from the amount adsorbed at a relative pressure of ~0.98 in the desorption branch. The micropore parameters were determined from the t-plot model. The following definitions were employed:

Mesopore volume:

$$V_{MESO}^{t-plot}\left(\frac{cm^3}{g}\right) = V_T - V_\mu^{t-plot} \tag{5}$$

Where V_T (cm^3/g) is the total pore volume and V_μ^{t-plot} is the corresponding micropore volume (cm^3/g) according to the t-plot model:

$$r(\text{Å}) = \left[\frac{13,99}{0,034-\log(\frac{p}{p_0})}\right]^{1/2} \tag{6}$$

External surface area:

$$S_{EXT}\ (m^2/g) = S_{BET} - S_\mu^{t-plot} \tag{7}$$

Where S_{BET} (m^2/g) is the specific surface area determined by the BET model and S_μ^{t-plot} is the corresponding micropore surface area for pores $\leq$ 20 Å, determined by the *t-plot* model.

2.5.3 Elemental analysis

CHN elemental analyses were carried out in a EuroVector 3000 CHNS analyzer. All analyses were done in duplicate to verify possible sample heterogeneity. For these materials, the relative standard deviation was <2%. The protocol consisted of weighing 2 mg of sample in a tin crucible using a 6-digit analytical balance (Mettler Toledo). Using an autosampler, the crucible was dropped into the analysis chamber and rapidly heated to ~1000 °C in the presence of an oxidation catalyst and oxygen. This process allows the organics to be completely decomposed into CO_2, H_2O and N_2. The so obtained gases were subsequently separated on a Porapak QS column at 80 °C and quantified with a TCD detector, using acetonitrile (99.9%) as an external standard.

2.5.4 X-Ray powder diffraction

Powder X-ray diffraction spectra were collected on a Bruker D8 powder X-ray diffractometer using CuKα radiation, λ=0.154056 nm. The spectra were recorded in the 2θ angle range of 5-50° with a step size of 0.02° and 3 seconds accumulation time.

2.5.5 Pyridine IR experiments

The FTIR spectroscopy measurements with pyridine as a probe molecule were carried out on a Vertex 70 Bruker spectrometer equipped with an MCT detector with a resolution of 2 cm^{-1}. All spectra were normalized to equal weight. A self-sustaining wafer of the sample was prepared, weighed and placed in a custom made quartz IR cell. Prior to the measurements, the sample was degassed at 500 °C for 1 h under high vacuum and a spectrum of the degassed sample was recorded to determine if all adsorbed water was removed. The sample mass, determined before the degassing step, was corrected for the amount of water present on the samples on the basis of the weight loss during the degassing treatment prior to the TCA-TPD procedure. The concentrations of Brønsted and Lewis acid sites were determined on the basis of quantitative *in-situ* IR studies. Excess of pyridine vapor sufficient to neutralize all acid sites was adsorbed at 170 °C under static conditions, followed by evacuation at the

11

same temperature to remove the gaseous and physisorbed pyridine molecules. This was tracked by evaluating the spectra on time. The band intensities in this spectrum were used to calculate the total concentration of Brønsted and Lewis sites. The total concentration of Brønsted and Lewis sites were calculated using the intensities of the 1545 cm^{-1} band, corresponding to pyridinium ions (PyH$^+$) and that at 1445 cm^{-1} band for pyridine coordinatively bonded to Lewis sites (PyL); and applying their respective extinction coefficients as 0.069 cm^2/μmol and 0.11 cm^2/μmol, respectively.

2.5.6 Structural infrared-spectroscopy

Prior to the FT-IR measurements, 2 g of the zeolite deactivated with humins was treated at room temperature in 100 ml of a 6 *wt.* % HF solution overnight to ensure complete dissolution of the zeolite, whereas the humins remain. Humins were collected from the solution by centrifugation and dried overnight at 80 °C in an oven. FT-infrared spectra were measured using a Perkin Elmer 2000 FT-IR spectrometer equipped with a ZnSe crystal, nitrogen-purged chamber, and an attenuated total reflection (ATR) unit with a single reflection diamond crystal. The resolution of the instrument was set to 4 cm^{-1} and the background of the clean crystal was measured. The absorbance spectra of the humin samples and background were recorded during 100 scans per spectrum.

3. Results and discussion

3.1 Zeolite deactivation

The proof of principle of the Fenton reactivation was evaluated on a ZSM-5 zeolite catalyst applied in the dehydration of *D*-glucose as model reaction, which is a relevant transformation in the field of lignocellulosic biomass valorization [32]. The as-received zeolite consists of polymorphic aggregates (Figure 1a) with a well-resolved MFI structure (Figure 1b) [33,34]. The N$_2$ physisorption isotherm (Figure 1c) shows a type I microporous material containing

meso/macropores (type IV) due to the interspace of the aggregates. The tensile strength effect (TSE) is clearly visible [35]. This material was calcined and used as a catalyst. Upon calcination, no relevant changes in the morphology and crystallinity were found; the micropore volume increased due to the removal of the NH_4^+ groups.

The reaction network for the dehydration of *D*-glucose proceeds via the conversion into 5-hydroxymethylfurfural (HMF), and ultimately into levulinic acid (LA) and formic acid (FA), Figure 2. These reactions are catalysed by Brønsted acid sites, and therefore a ZSM-5 containing Brønsted sites was chosen. During the reaction, an insoluble by-product denoted as humins is formed [36]. The restricted pore network of ZSM-5, with pores of 5.3 x 5.6 Å and 5.1 x 5.5 Å [34], makes humins removal a non-trivial process, as deposits are formed both outside and inside of such narrow pores. The reaction conditions employed are similar to those reported by Patil *et al.* [37].

The organics deposition over ZSM-5 was studied along the reaction time. Following recovery, the spent zeolites were dried and characterized by TGA (Figure 3). Figure 3A represents the TGA relative patterns with the corresponding DTGA at the bottom (Figure 3B). Virgin ZSM-5 (AP27-F) shows water desorption that is gradually released as the temperature rises to ~200 °C (Figure 3B). The weight loss between 200 and 900 °C is due to dehydroxylation given as:

$$2\ Si(Al)\text{-}OH \rightarrow Si(Al)\text{-}O\text{-}Si(Al) + H_2O \qquad (8)$$
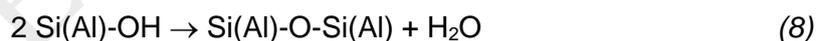
This process accounts for 1.4 *wt.*% mass loss. Figure 3 also shows the behaviour of the zeolites following glucose dehydration at various reaction times. Two distinct regions can be distinguished, which can be better seen in the DTGA graphs (Figure 3B). The region between 30 and 200 °C represents the mass loss resulting from water desorption. The broad region between 200 and 900 °C embodies the weight loss caused by the organic decomposition plus dehydroxylation; the latter is considered equal to the fresh zeolite, *i.e.* accounting for 1.4 *wt.*%. From the patterns, the organics start to decompose at 200 °C with a maximum between 375 and 450 °C, and the complete decomposition requires temperatures between 600 and 650 °C.

13

The DTGA provides evidence of a secondary effect; the increase in the organics content is accompanied by a decrease of the physisorbed water. This is due to the increased hydrophobicity of the zeolite from the humins (that are insoluble in water), and therefore less adsorption capacity on the zeolite surface becomes available. The second effect is the depletion of the surface area itself.

The organic content in the zeolite increases linearly with the reaction time (inset in Figure 3B). For the final 6h-sample, the TGA result was verified by elemental carbon analysis; this confirmed a carbon content of 5.36 *wt.*% (Table 1). Fouling was confirmed from the N_2 physisorption isotherms with a noticeable reduction of the adsorption capacity in the complete isotherm in Figure 4. Quantitatively, Table 1 compiles the textural parameters; a considerable depletion of the surface area from 307 m^2/g for the fresh zeolite, decreasing to 89 m^2/g for the deactivated zeolite was found. That corresponds to a loss of 70% of the surface area. Similarly, the pore volume decreased around 60%. The acid site density as determined by pyridine IR helped to understand the zeolite deactivation pathway (Table 1). The Brønsted and Lewis sites are reduced by 36 % and 65 % respectively, when referenced to the fresh counterpart. Therefore, while both surface area and acidity are decreased, the active-site accessibility - which is provided by the porous structure - has been more severely affected than the acidity properties in the spent catalyst.

It is then concluded that after 6 h reaction time, the catalyst is significantly fouled, with a drop in the relevant properties; surface area, pore volume and acid site density. This deactivation protocol was used for the proceeding reactivation studies.

In order to produce sufficient amount of deactivated catalyst, the reaction was scaled 15-fold up. A similar concentration of organics was obtained after scaling up. The TGA is shown in Figure S-2 of the supporting information.

3.2 Organic deposits characterization

Infrared spectroscopy was used to evaluate the approximate chemical structure of the organic deposits [37-41]. Figure 5 shows the IR spectra of the organics formed during the dehydration of *D*-glucose catalysed by sulphuric acid (Figure 5-A) and ZSM-5 (Figure 5-B). The spectra in both cases are quite similar, despite the spatial limitations imposed by the zeolite as compared to the sulphuric acid. They present comparable bands with slight differences in the relative intensity of some bands. Both spectra exhibit a similar general pattern as those reported for the glucose-derived humins [37,38], indicating a similar chemical nature. The broad band centred at around 3400 cm^{-1} can be ascribed to the stretching vibration of O-H of alcohols [38]. The bands in the region of 2850-2950 cm^{-1} correspond to aliphatic C-H stretch, whereas the intense band at 1700 cm^{-1} could be assigned to the C=O stretch corresponding to ketones, aldehydes, esters and acids [38,40]. The bands in the 1000–1450 cm^{-1} region are assigned to C-O stretching and O-H bending vibrations [40]. Specifically, the contribution at around 1200 cm^{-1}, whose relative intensity is slightly higher for the H_2SO_4-formed humin is attributed to the C-O-C stretching [41]. Higher intensities of both 1200 cm^{-1} and broad O-H band (more hydrogen bonded species) can point to the higher contribution of alcohol derivatives in the case of humins formed by H_2SO_4. On the other hand, the 1700 cm^{-1} (ketones, aldehydes) and 1600 cm^{-1} bands (organic acid, esters, salts) are of higher intensity for the zeolite what can suggest their higher concentration in the case of zeolite catalysed process. Some bands can be ascribed to substituted furan rings such as the ones centred at 1620 and 1510 cm^{-1}, attributed to C=C vibrations [40], as well as the bands in the region at 875–750 cm^{-1}, which are assigned to aromatic C-H out-of-plane bending vibrations [38,40]. The IR spectrum interpretation of the ZSM-5 derived organic deposit is consistent with the molecular structure proposed by van Zandvoort and co-workers [38] for the humins formed during the acid-catalyzed dehydration of glucose. This consists of a furan-rich polymer network containing different oxygen functional groups.

3.3 Catalyst reactivation

Deactivated ZSM-5 catalyst was subjected to the oxidative reactivations. The DTGA patterns (Figure 6) evidence, at qualitative basis, that humins are removed by this treatment at 70 °C and 90 °C; the DTGA shows a nearly humin-free pattern. TGA results were further verified with elemental carbon analysis and the regeneration efficiency was determined (η^R, Table 1). This parameter provides a more precise understanding of the regeneration efficiency, since it is selective to the carbon content. At 70 °C the efficiency was 76% while at 90 °C it raised up to 96 %, which is an expected kinetic trend with temperature. Non-Fenton H_2O_2 experiments, *i.e.* without Fe(III)-nitrate, revealed that this approach works well with efficiencies of 70% and 97%, at 70 °C and 90 °C respectively. Interpretation of this result can be found in: 1) the H_2O_2 oxidation potential (1.77 V) [42] can be sufficient to oxidize the humins at 90 °C, despite the $^\bullet$OH higher oxidation potential, and 2) the parent zeolite contains Fe from the manufacturing process (*ca.* 470 ppm as determined by ICP); this level of Fe can catalyse the production of $^\bullet$OH via a heterogeneous Fenton reaction pathway [43]. The possible oxidative mechanistic routes for this industrial zeolite reactivation are schematically illustrated in Figure 7, which represents various oxidative reaction pathways: the homo-, heterogeneous $^\bullet$OH generation routes as well as the direct H_2O_2 oxidation. For this case study, the addition of Fe is beneficial at low temperatures, 70 °C, with a higher removal efficiency. However, the similar efficiency at 90 ºC obtained in the absence or presence of the homogeneous Fe salt, could be explained bearing in mind that the catalyst loading is a critical factor involved in the removal efficiency, as showed in previous works for the degradation of pollutants in wastewaters [44-46]. It is said that if the catalyst loading in the aqueous solution exceeds the optimum range, the generated $^\bullet$OH would be consumed by the excess of catalyst ($Fe^{2+} + ^\bullet OH \rightarrow Fe^{3+} + OH^-$). Hence, it is postulated that the quantity of Fe catalyst provided by the impurities of the zeolite, would be enough to catalyse the degradation process at that temperature, so that the excess of Fe salt added in the homogeneous process does not have any beneficial impact on the degradation

efficiency. Other critical factor is the H_2O_2 dosage, which must be adjusted to avoid the invalid decomposition/consumption of H_2O_2/$^•OH$ and the oxidation of ferrous ions. Moreover, the radicals can be decomposed on the zeolite walls. The effect of the Fe concentration and the oxidant amount at 90 ºC was further investigated (Table S-1). As indicated in the table, the effect of Fe can even be negative in the regeneration efficiency. Nonetheless, it should be noted that most of the discussed literature focus on the waste-water treatments, where the pollutants are present in the water medium; however, in our case the molecule to degrade (humins) is embedded inside of the porous structure of the zeolite. Our understanding is that by adding more Fe, the Fenton kinetics could be expected to be faster but the radicals could not diffuse at the same rate through the zeolite crystals due to the mass transfer limitations of the ZSM-5 pore size. Overall, the long diffusional lengths in the zeolite is an obstacle due to the short life time of the OH radicals. Therefore, the mass transfer diffusional control in crystalline zeolites is an obstacle for the penetration of the radicals. That means that having a mild Fenton kinetics with a slower production of radicals is more beneficial.

From a fundamental stand point, the preparation of a Fe-free ZSM-5 would clarify whether additional Fe is required. However, the Fe concentration in the homogeneous protocol is very small without affecting the Brønsted capacity of the treated zeolite (as will be shown later). Therefore, in practical terms, the homogeneous route is a more sensible approach, while a non-Fenton experiment will serve as a proper reference.

Another contribution to the removal efficiency can come from the phenomenon of physical wash out; whether the liquid medium itself can wash out the humins physically. To understand the extent to which this occurs, a control experiment was carried out in which the fouled zeolite was treated in hot water at 90 °C. The DTGA profile shows that a fraction of humins have been removed (Figure 6); the carbon analysis confirms that only 17% of the humins was extracted. This fraction would correspond to the water-soluble oligomers or loosely adsorbed humins. In

conclusion, the Fenton or non-Fenton H_2O_2 oxidation treatments are highly efficient, much more than a water-treatment, to extract and decompose the humins from ZSM-5.

3.4 Properties of the reactivated materials

The reactivated catalytic materials were characterised by a number of physico-chemical techniques to evaluate the effect of the treatment on the structural and textural features. XRD analysis was performed to evaluate possible changes in the crystal structure. The XRD patterns given in Figure 8 of the regenerated materials at 90 °C coincide closely with that of the as-received zeolite, both in crystallinity and lattice dimension. The 20-25° magnification shows this clearly (inset Figure 8). Therefore, the regeneration conditions do not affect the crystal structure of the catalyst nor the crystallinity. This is particularly notable because of the acidic medium and chelating agents (formats and oxalates) produced under the Fenton reactions. These conditions may disaggregate the zeolite by leaching Al(III) out of the structure and distort the crystal structure. As it will be seen later, the acidity is neither been reduced.

The catalysts' texture was evaluated by N_2 gas adsorption. The isotherms (Figure 4) of the fresh, spent, and regenerated catalysts reveal few moderate changes in the texture. Adsorption capacity is seen to increase following regeneration treatment, coming close to that of the fresh ZSM-5. This confirms the removal of humins from within the structure, unblocking the external pore mouths and intra-crystalline channels, thereby allowing access to substrate. All reactivation treatments resulted in a three-fold increase in BET surface area as compared to the deactivated material. Compared to the fresh ZSM-5, the BET surface area is about 13-18% lower. Closer inspection of the textural parameters (Table 1) reveals that the mesopore volume is 7-11% lower whereas the micropore volume is 14-16% lower than the fresh ZSM-5. This suggests that the remaining humins are located preferentially within the zeolite micropores. This observation may be explained by a combination of effects: the limited life time of the $^\bullet OH$ species and the small pore dimensions which impose mass transfer and thereby

accessibility limitations of the $^{\bullet}$OH into the zeolite crystals. This will result in $^{\bullet}$OH chemical and physical recombination processes, limiting the complete oxidation of the most occluded humins. Despite that, the remaining humins was not an obstacle for the activity recovery, as it will be discussed below.

The acidity features were evaluated by pyridine-adsorbed FTIR spectroscopy (Table 1). The fresh zeolite contains both Brønsted (542 μmol/g) and Lewis sites (107 μmol/g). The Brønsted sites are reduced by 36% whereas the Lewis sites diminished by 65%, ascribed to the deposition of humins. These values are increased when the materials are treated at 70 °C in Fenton or non-Fenton H_2O_2 treatment. It is particularly remarkable that the density of both sites is higher for the non-Fenton H_2O_2 material than the fresh counterpart; 10 % higher for the Brønsted and 50% higher for the Lewis sites. This could be explained by 1) the removal of amorphous domains (invisible to XRD) during the treatment, rendering a material with a higher intrinsic acidity and 2) due to the Al-dislodgement forming framework connected hexa-coordinated Al [47]. In the case of the Fenton treatment (AP27-Fe70), similar acidity value as for the fresh ZSM-5 was found. The lower values as compared to the AP27-Pe70 can be ascribed to the Fe(III)-exchange on the Brønsted and Lewis sites that would reduce the acidity; therefore this would counterbalance the positive effect seen under the non-Fenton H_2O_2 treatment. The materials treated at 90 °C were routinely characterised by NH_3 TPD and compared to the 70 °C and fresh zeolite; similar trends to the 70 °C treated materials as discussed for the pyridine data were observed.

The reactivated materials were evaluated in the dehydration of *D*-glucose. Figure 9 represents the conversion profiles of the fresh and 70 °C treated catalysts. The fresh zeolite seems to be faster initially but the conversion after 6 h was comparable for all of them with slight differences of ± 3%. Therefore, both mild reactivation procedures (Fenton and non-Fenton H_2O_2) are effective in recovering the catalyst activity. It must be kept in mind that the reactivated materials

19

at 70 °C still contain around 24-30% of the humins but this does not affect the intrinsic activity of the acid sites for this reaction. The materials treated at 90 ºC showed similar conversion profiles (not shown for clarity) than those obtained with the treated-catalyst at 70 ºC, despite the humins content is significantly lower in the former. We think that the remaining humins are those embedded within the core of the zeolite crystals while the reaction takes place on the more outer side of the crystal. This is in agreement with the well-known Al-zoning in ZSM-5 [48]. The experimental data show that the humins grow inside the zeolite, reducing the surface area and pore volume. However, as there is no strong evidence where the reaction takes place, we prefer not to speculate on this matter presently. Therefore, application of the lower processing temperature would suffix in terms of activity recovery with savings in operational costs.

4. Conclusions

Fenton chemistry-derived $^{\bullet}$OH species, and H_2O_2, have been effective as oxidizing agents to remove the humins deposited on a ZSM-5 zeolite porous catalyst during the *D*-glucose dehydration reaction. These oxidative processes have been conducted at 70 and 90ºC, and reactivation was highly effective in terms of removal of the organics as well as recovery of the initial catalytic activity. The properties of the reactivated zeolites were preserved, with similar structural and textural features and improved acidity. Hot water extraction was ineffective to remove the humins from ZSM-5, which confirmed the crucial role of H_2O_2 in the regeneration mechanism. Insights about the mechanism were discussed, with the conclusion of not being able to discriminate between a homogeneous or a heterogeneous mechanism, or direct H_2O_2, or a combination of them, due to the presence of Fe impurities in the zeolite structure. The impurities' role is generally overlooked in scientific discussions when dealing with commercial catalysts. From the methodology point of view, a hot water reference experiment may be done first to decide whether an oxidative approach is worthwhile. In conclusion, catalyst

20

regeneration can be carried out at very mild conditions through an environment-friendly approach with highly satisfactory results.

References

[1]   C.H. Bartholomew, Appl. Catal. A: Gen. 212 (2001) 17–60.

[2]   M. V. Twigg, M.S. Spencer, Appl. Catal. A: Gen. 212 (2001) 161-174.

[3]   M.D. Argyle, C.H. Bartholomew, Catalysts 5 (2015) 145-269.

[4]   J.A. Moulijn, A.E. van Diepen, F. Kapteijn, Appl. Catal. A: General 212 (2001), 3-16.

[5]   A.A. Lappas, M. C. Samolada, D. K. Iatridis and S. S. Voutetakis, Fuel 81 (2002) 2087-2095.

[6]   M. Guisnet, F.R. Ribeiro, Deactivation and Regeneration of Zeolite Catalysts, Hutching, G. J. Ed.; Imperial College Press, 2011.

[7]   R.G. Copperthwaite, G.J. Hutchings, P. Johnston, S.W. Orchard, J. Chem. Soc., Faraday Trans. 82 (1986) 1007-1017.

[8]   S. Khangkham, C. Julcour-Lebigue, S. Damronglerd, C. Ngamcharussrivichai, M.H. Maneroa, H. Delmas, Appl. Catal. B: Environ. 140-141 (2013) 396-405.

[9]   Y. Fan, Y. Cai, X. Li, H. Yin, L. Chen, S. Liu, J Anal. Appl. Pyrol. 111 (2015) 209-215

[10] L.Y. Jia, Al Farouha, L. Pinard, S. Hedan, J.-D. Comparot, A.Dufour, K.B. Tayeb, H. Vezin, C.Batiot-Dupeyrat, Appl. Catal. B: Environmental 219 (2017) 82-91.

[11] R. Bauer, G. Waldnera, H. Fallmann, S. Hager, M. Klare, T. Krutzler, S. Malato, P. Maletzky, Catal. Today 53 (1999) 131–144.

[12] Venny, S. Gan, H.K. Ng, Chem. Eng. J. 213 (2012) 295–317.

[13] J. de Laat, J.; T.G. Le, Appl. Catal. B Environ. 66 (2006) 137-146.

[14] I. Melian-Cabrera, S. Espinosa, F.J. Garcia-Montelogo, F. Kapteijn, J.A. Moulijn, Chem. Commun. (2005) 1525-1527.

[15] I. Melian-Cabrera, F. Kapteijn, J.A. Moulijn, Chem. Commun. (2005) 2744-2746.

[16] I. Melian-Cabrera, F. Kapteijn, J.A. Moulijn, Catal. Today 110 (2005) 255-263.

[17] M. J. Ortiz-Iniesta, I. Melián-Cabrera, Microp. Mesop. Mat. 206 (2015) 58-66.

[18] L.L. Perez, M.J. Ortiz-Iniesta, Z. Zhang, I. Agirrezabal-Telleria, M. Santes, H.J. Heeres, I. Melian-Cabrera, J. Mater. Chem. A 1 (2013) 4747-4753.

[19] Z. Zhang, D.L. Santangelo, G. ten Brink, B.J. Kooi, J.A. Moulijn, I. Melian-Cabrera, Mater. Lett. 131 (2014) 186-189.

[20] Z. Zhang, I. Melián-Cabrera, J. Phys. Chem. C 118 (2014) 28689-28698.

[21] Z. Zhang, A. Mayoral, I. Melian-Cabrera, Micropor. Mesopor. Mat. 220 (2016) 110-119.

[22] Y. Xia, R. Mokaya, J. Phys. Chem B 110 (2006) 9122-9131.

[23] J. Kecht, T. Bein, Micropor. Mesopor. Mater. 116 (2008) 123-130.

[24] N. Alam, R. Mokaya, J. Mater. Chem. 18 (2008) 1383-1391.

[25] F. Fan, Z. Feng, K. Sun, M. Guo, Q. Guo, Y. Song, W. Li, C. Li, Angew. Chem. Int. Ed. 48 (2009) 8743-8747.

[26] P. Wang, D. Yang, J. Hu, J. Xu, G. Lu, Catal. Today 212 (2013) 62.e1–62.e8.

[27] Wu, J. Liao, S. Fang, A.S.T. Chiang, Adsorption 16 (2010) 69-74.

[28] S. Wang, H. Li, S. Xie, S. Liu, L. Xu, Chemosphere 65 (2006) 82-87.

[29] I. Braschi, S. Blasioli, E. Buscaroli, D. Montecchio, A. Martucci, J. Environ. Sci. 43 (2016) 302-312.

[30] C.A. Chiu, K. Hristovski, S. Huling, P. Westerhoff, Water Res. 47 (2013) 1596-1603.

[31] Z. Tang, Physicochemical Treatment of Hazardous Wastes, CRC Press, 2003.

[32] Z. Xue, M.G. Ma, Z. Li, T. Mu, RSC Advan.6 (2016) 98874-98892.

[33] M.M.J. Treacy, J.B. Higgins, Collection of Simulated XRD Powder Patterns for Zeolites, Elsevier, Amsterdam, 2001.

[34] URL: http://europe.iza-structure.org/IZA-SC/material_tm.php?STC=MFI (Accessed on 22/2/2018)

[35] J.C. Groen, J. Pérez-Ramírez, Appl. Catal. A: Gen. 268 (2004) 121-125.

[36] B. Girisuta, Levulinic acid from lignocellulosic biomass, University of Groningen PhD dissertation, 2007, URL: http://www.rug.nl/research/portal/files/10230666/thesis.pdf (Accessed on 22/2/2018).

[37] S.K.R. Patil, J. Heltzel, C.R.F. Lund, Energy Fuels 26 (2012) 5281-5293.

[38] I. van Zandvoort, Y. Wang, C.B. Rasrendra, E.R.H. van Eck, P.C.A. Bruijnincx, H.J. Heeres, B.M. Weckhuysen, ChemSusChem 6 (2013) 1745-1758

[39] S.K.R. Patil, C.R.F. Lund, Energy Fuels. 25 (2011) 4745-4755.

[40] M. Sevilla, A. B. Fuertes, Chem. Eur. J. 15 (2009) 4195-4203.

[41] J. Ryu, Y. Suh, D.J. Suh, D. J. Ahn, Carbon 48 (2010) 1990-1998.

[42] M.A. Tarr in Chemical Degradation Methods for Wastes and Pollutants: Environmental and Industrial Applications (Environmental Science & Pollution), 1st ed., CRC Press, 2003.

[43] E.V. Kuznetsova, E.N. Savinov, L.A. Vostrikova, V.N. Parmon, Appl. Catal. B: Environ. 51 (2004) 165-170.

[44] N. Wang, T. Zheng, G. Zhang, P. Wang, J. Environ. Chem. Eng. 4 (2016) 762-787

[45] N. Wang, Q. Zhao, A. Zhanf, RSC Advan.7 (2017) 27619-27628.

[46] N. Wang, T. Zheng, J. Jiang, W. Lung, X. Miao, P. Wang, Chem. Eng. J. 239 (2014) 351–359

[47] I. Melián-Cabrera, E.R.H. van Eck, S. Espinosa, S. Siles-Quesada, L. Falco, A.P.M. Kentgens, F. Kapteijn, Jacob A. Moulijn, Appl. Catal. B: Environ. 203 (2017) 218-226.

[48] R. von Ballmoos, W.M. Meier, Nature 289 (1981) 782–783.

Figures and Tables

Table 1. Physico-chemical characterisation of the ZSM-5 catalysts.

Material	Treatment	C (*wt.%*)	η^R (%) [a]	Pyridine IR (µmol/g) [b,c]	S_{BET} (m²/g)	V_T (cm³/g)	V_μ (cm³/g)	V_M (cm³/g) [e]
AP27-F	Fresh, activated	-	-	542, 107 (1.00)	307	0.168	0.101	0.067
AP27-D [f]	Deactivated	5.36	0	345, 37 (-) [d]	89	0.062	0.033	0.029
AP27-Pe70 [g]	H_2O_2, 70 °C	1.60	70	595, 160 (1.05)	268	0.153	0.087	0.067
AP27-Fe70 [h]	Fenton, 70 °C	1.31	76	542, 103 (0.95)	252	0.149	0.086	0.063
AP27-Pe90 [g]	H_2O_2 at 90 °C	0.15	97	(1.07)	268	0.156	0.085	0.071
AP27-Fe90 [h]	Fenton, 90 °C	0.20	96	(0.94)	266	0.156	0.086	0.070
AP27-W90	H_2O at 90 °C	4.44	17	-	-	-	-	-

a. Regeneration efficiency defined as: $\eta^R = \left(1 - \frac{C^{REG}}{C^{AP27-F}}\right)$, where C^{REG} is the carbon concentration of the regenerated material and C^{AP27-D} for the deactivated zeolite; **b.** Brønsted followed by Lewis sites concentrations; **c.** Values in parenthesis corresponds to the NH_3 adsorption TPD, relative to the fresh AP27-F; **d.** NH_3 TPD cannot be done on this sample due to the presence of humins; **e.** $V_M = V_T - V_\mu$; **f.** Spent catalyst after *D*-glucose dehydration (0.125 M *D*-Glucose, 0.15 g of activated ZSM-5 at 180 °C); **g.** the sample code Pe refers to peroxide; **h.** the sample code Fe refers to Fenton.

25
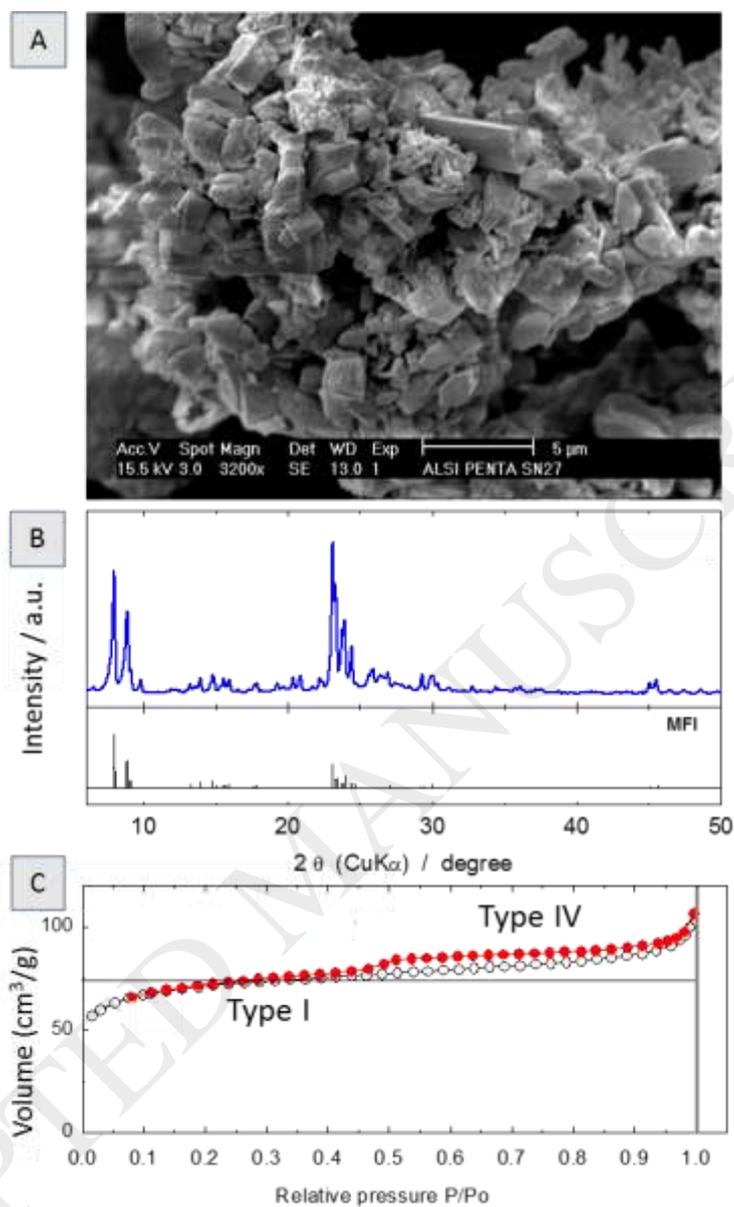
Figure 1. Structural and textural features of the ZSM-5: **A**) SEM image; **B**) XRD pattern, including the simulated XRD pattern for a MFI structure (some unknown reflections were observed, due to impurities coming from the manufacturing process) and **C**) N_2-physisoprtion isotherm of the NH_4-form zeolite. The mesoporosity gives rise to a hysteresis loop with a closure point at p/po~0.42 due to the TSE effect.
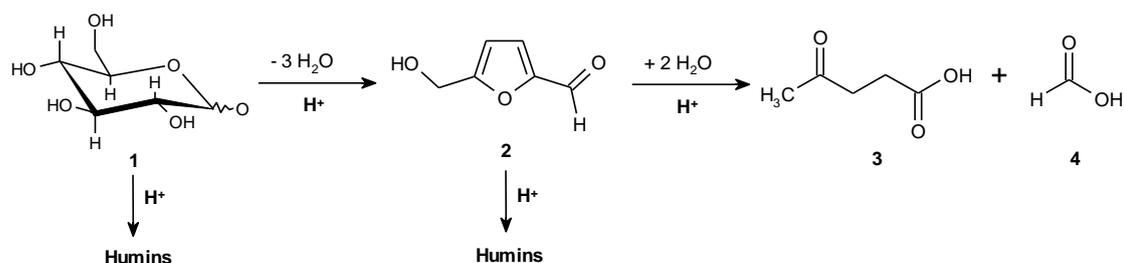
Figure 2. Dehydration of *D*-glucose (**1**) into 5-(hydroxymethyl)furfural (**2**), levulinic acid (**3**) and formic acid (**4**). Humins are produced as by-products.
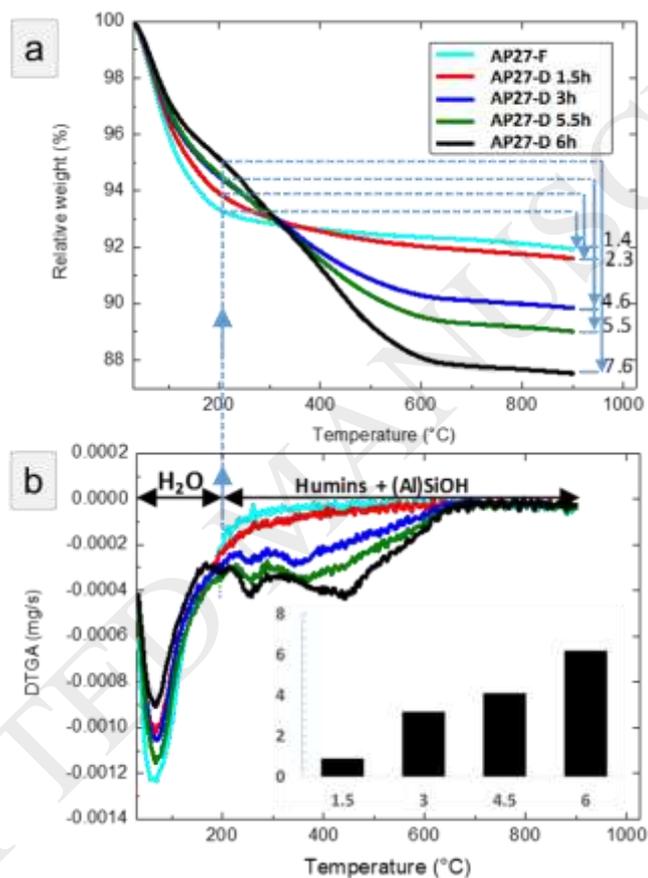
Figure 3. Thermogravimetric analysis in air of ZSM5 after *D*-glucose dehydration. The relative weight loss (**top**) and corresponding DTGA (**bottom**) curves of the fresh zeolite (AP27-F) and spent catalysts for various reaction times (AP27-**X**h, where **X** is the reaction time in h). The number at the end of each TGA pattern corresponds to the weight loss between 200 and 900 °C. Such a weight loss corresponds to humins plus dehydroxylation water; the latter is ~1.4 *wt*.% as deduced from the fresh zeolite (AP27-F). The humins concentration is then calculated by the difference between the weight loss minus 1.4 *wt*.%. In theory the amount of hydroxyls should not be affected by the deposition of humins, since it is a physical adsorption process of the later ones. The inset graph in the bottom corresponds to the humins concentration (*wt*.%) as a function of the reaction time (h).
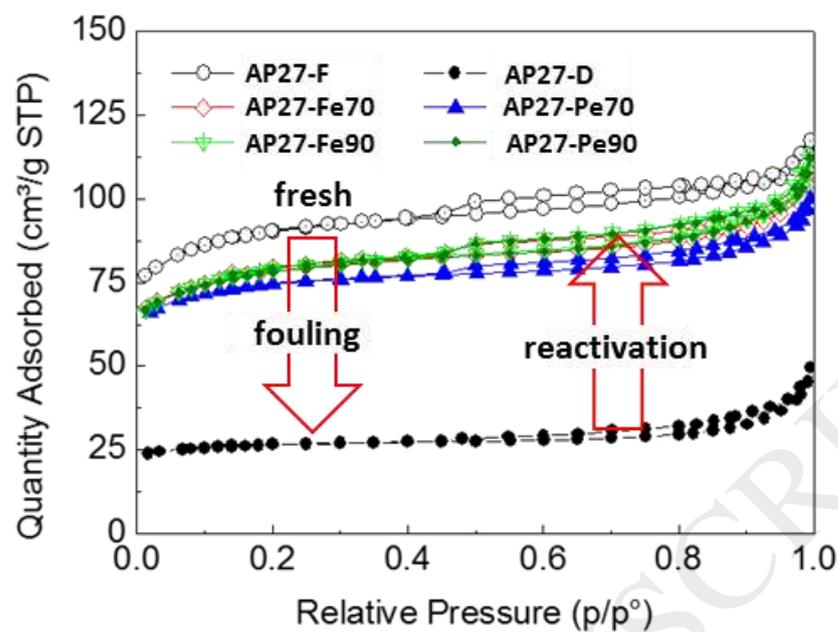
Figure 4. N$_2$ physisorption isotherms of the H-ZSM5: fresh (AP27-F), deactivated (AP27-D) and after various regeneration procedures, as summarized in Table 1.
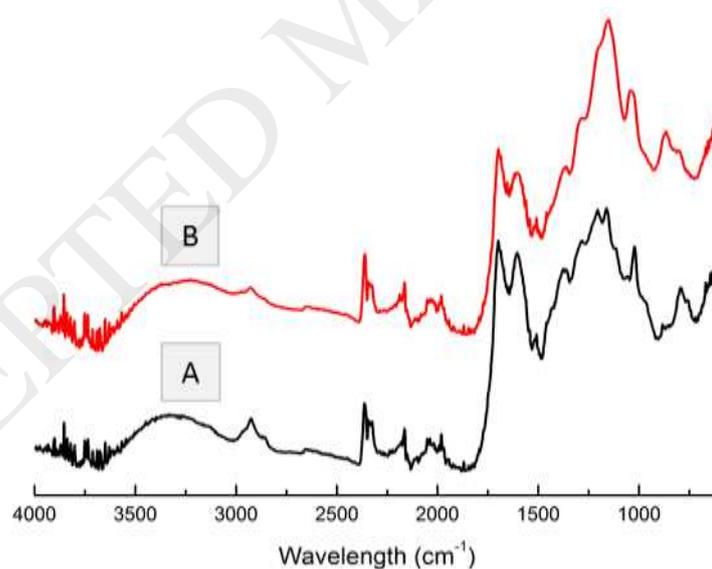
Figure 5. IR spectra of humins recovered after glucose dehydration, 0.125 M glucose for 6 h at 180 °C. IR spectra of: **A**) humins formed using ZSM-5; **B**) humins formed using H$_2$SO$_4$.
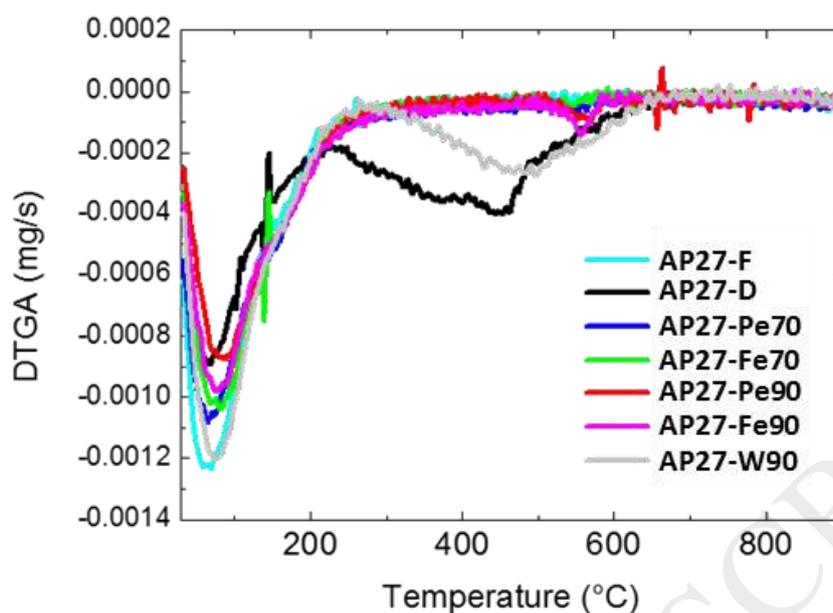
Figure 6. DTGA analysis of deactivated H-ZSM5 zeolite (AP27-D) and after various regeneration procedures. Fresh zeolite (**AP27-F**) is included for comparison. Raw TGA patterns can be found in Figs. S-2, S-3 and S-4, in the electronic supporting information.
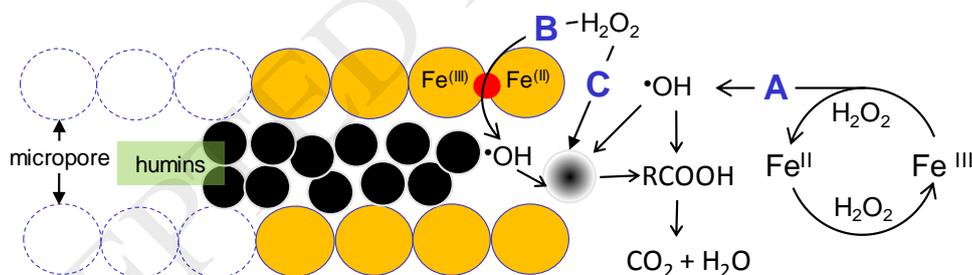
Figure 7. Possible reaction pathways of the H_2O_2 or Fenton oxidative degradation of humins fouling a microporous ZSM-5 zeolite after *D*-glucose dehydration. Three mechanistically distinct routes for the $^\bullet OH$ radical's production can be occurring: **A)** homogeneous via externally added Fe-salt; **B)** heterogeneously catalysed by the Fe traces present in the zeolite, and **C)** direct non-Fenton H_2O_2 based oxidation.
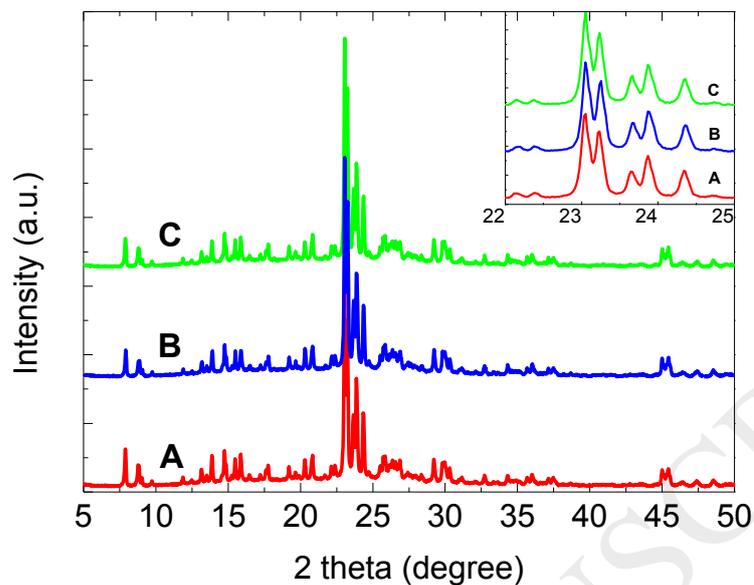
Figure 8. XRD patterns: **A)** AP27-F, **B**) AP27-Pe90 and **C**) AP27-Fe90. Inset is a magnification in the 22-25 degree (2 theta) region.
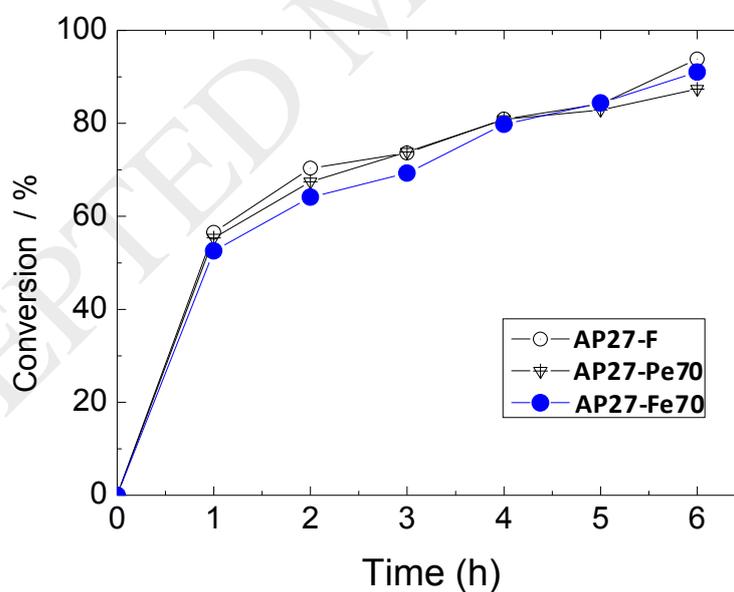
Figure 9. *D*-Glucose conversion as a function of the reaction time: 0.125 M D-Glucose, 0.15 g of activated ZSM-5 at 180 °C: fresh (**F**), and after various reactivation at 70 °C, under non-Fenton H_2O_2 (**Pe70**) and Fenton (**Fe70**).

30